Delft University of Technology

Aerodynamic Optimisation of Acoustic Liners

Shahzad, H.; Hickel, S.; Modesti, D.

DOI
10.2514/6.2024-3282

Publication date
2024

Document Version
Final published version

Published in
30th AIAA/CEAS Aeroacoustics Conference (2024)

Citation (APA)
Shahzad, H., Hickel, S., & Modesti, D. (2024). Aerodynamic Optimisation of Acoustic Liners. In *30th AIAA/CEAS Aeroacoustics Conference (2024)* Article AIAA 2024-3282 (30th AIAA/CEAS Aeroacoustics Conference, 2024). https://doi.org/10.2514/6.2024-3282

Important note
To cite this publication, please use the final published version (if applicable).
Please check the document version above.

Copyright
Other than for strictly personal use, it is not permitted to download, forward or distribute the text or part of it, without the consent of the author(s) and/or copyright holder(s), unless the work is under an open content license such as Creative Commons.

Takedown policy
Please contact us and provide details if you believe this document breaches copyrights.
We will remove access to the work immediately and investigate your claim.

This work is downloaded from Delft University of Technology.
For technical reasons the number of authors shown on this cover page is limited to a maximum of 10.

Green Open Access added to TU Delft Institutional Repository

'You share, we take care!' - Taverne project

https://www.openaccess.nl/en/you-share-we-take-care

Otherwise as indicated in the copyright section: the publisher is the copyright holder of this work and the author uses the Dutch legislation to make this work public.

Aeroacoustics Conferences
June 4-7, 2024, Rome, Italy
30th AIAA/CEAS Aeroacoustics Conference (2024)

10.2514/6.2024-3282

Check for updates

Aerodynamic Optimisation of Acoustic Liners

Haris Shahzad, Stefan Hickel and Davide Modesti
Aerodynamics Group, Faculty of Aerospace Engineering, Delft University of Technology, Kluyverweg 2, 2629 HS Delft, The Netherlands

We present pore-resolved direct numerical simulations (DNS) of turbulent flows grazing over acoustic liners with aerodynamically and/or acoustically optimised orifice configurations. Our DNS explore a large parameter space, studying different families of orifice geometries including the influence of orifice shape, orientation, and number. All flow cases show an increase in drag compared to the smooth wall. However, the added drag can be reduced by as much as ~60%, as compared to conventional acoustic liners by simply changing the shape of the orifice or the orientation in the case of a non-circular orifice. Complementary acoustic simulations show that this drag reduction can be achieved while retaining the same noise reduction properties.

Downloaded by Technische Universiteit Delft on July 16, 2024 | http://arc.aiaa.org | DOI: 10.2514/6.2024-3282

I. Introduction

Aircraft engines are the primary source of noise during take-off and landing. To reduce noise, engine nacelles are equipped with noise control devices called acoustic liners. Acoustic liners are simple devices, and their working mechanism is based on the idea of dissipating noise by tuning their resonance frequency with the dominant frequency of the engine fan. They have the potential to attenuate noise by as much as 8–10dB and are thus, required on all aircraft jet engines. Acoustic liners have been optimised primarily from an acoustic perspective [1–4]. From an aerodynamic perspective, however, they behave like surface roughness and contribute to an increase in aerodynamic drag. This aerodynamic penalty has been accepted as a necessary compromise. The objective of the current study is to show that it is possible to reduce this aerodynamic penalty while maintaining or improving acoustic noise attenuation.

The effect of acoustic liners on the background turbulent flow has only been studied recently, both using experiments [5–8] and numerical simulations [9, 10]. Experimental studies are often characterized by large uncertainties in drag measurements, and numerical simulations of such surfaces are computationally very expensive. Therefore, most studies have used simplifying assumptions to make the problem more approachable with numerical simulations. As a result, estimates of the added drag reported in the literature have a massive spread, ranging from 3% up to 500%, depending on the numerical or experimental technique that was used. Our group recently performed the first Direct Numerical Simulations (DNS) of fully resolved acoustic liner geometries [11]. Our analysis related the added drag to the wall-normal velocity fluctuations and the wall-normal Forchheimer permeability of the plate. Building on these findings, we showed that it is possible to predict the added drag of acoustic liners in operating conditions [11, 12].

Copyright © 2024 by the American Institute of Aeronautics and Astronautics, Inc. All rights reserved.

Downloaded by Technische Universiteit Delft on July 16, 2024 | http://arc.aiaa.org | DOI: 10.2514/6.2024-3282

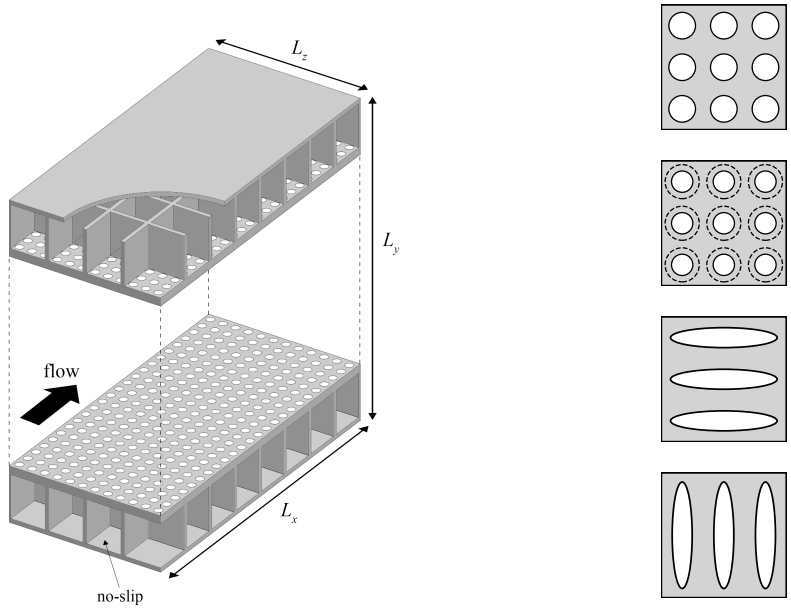

Fig. 1 Sketch of the computational domain. Turbulent channel flow configuration with box dimension $L_x \times L_y \times L_z = 3\delta \times 2(\delta + h) \times 1.5\delta$. The orifice shape is altered to investigate its influence and some of the configurations are shown on the right.

Hence, we are confident that better aerodynamic performance can be achieved by finding plate geometries that reduce the wall-normal velocity fluctuations induced by the orifices.

Howerton and Jones [13] studied different orifice configurations, changing the orifice shape and orientation, including rectangular orifices either parallel or perpendicular to the flow, and found that the perpendicular slot orifice performed better compared to the baseline circular orifices. The parallel slot orifice, on the other hand, despite having the same dimensions as the perpendicular slot orifice, had the highest added drag (at a freestream Mach number $M = 0.3$). Furthermore, Howerton and Jones [13] noted that, despite changes in the orifice shape, the acoustic performance was largely unchanged, meaning that there is potential for reducing the added drag, without hampering the acoustic attenuation properties.

To the best of our knowledge, acoustic liners with varying orifice configurations have been studied only experimentally by Howerton and Jones [13] and the physical rationale behind their choice of orifice configuration was missing. In this work, we use our recent findings [11] on scaling laws for the added drag to devise optimized acoustic liner geometries that reduce the added drag while having the same acoustic performance as the baseline configuration.

Downloaded by Technische Universiteit Delft on July 16, 2024 | http://arc.aiaa.org | DOI: 10.2514/6.2024-3282

	Re_b	Re_τ	d_x^+	d_z^+	$K/t^2 \times 10^3$	$1/(\alpha t)$	Δx^+	$\Delta y^+_{\min}$	Δz^+	N_x	N_y	N_z	ΔU^+	$C_f \times 10^3$
S	9268	506.1	0	0	-	-	5.1	0.80	5.1	300	350	150	-	5.96
L-S	8264	505.3	40.4	40.4	6.33	0.127	1.5	0.80	1.5	1000	500	500	1.90	7.33
L-T	8492	515.8	33.0	33.0	17.0	0.156	1.3	0.81	1.3	1200	600	500	0.88	6.86
L-E_{x-3}	6562	492.8	29.6	157.7	7.32	0.0869	5.9	0.79	1.1	250	500	700	4.56	10.7
L-E_{x-6}	7801	501.5	15.0	160.5	2.23	0.0401	6.0	0.80	0.6	250	500	1300	1.95	7.84
L-E_{x-9}	8650	515.5	10.3	165.0	1.07	0.0217	6.2	0.82	0.4	250	500	2000	0.51	6.52
L-E_{z-3}	8052	510.0	163.2	30.6	7.32	0.0869	1.1	0.82	6.1	1400	500	125	1.92	7.62
L-E_{z-6}	8021	506.8	162.1	15.2	2.23	0.0401	0.6	0.81	6.1	2600	500	125	1.80	7.57
L-E_{z-9}	8335	515.6	165.0	10.3	1.07	0.0217	0.4	0.82	6.2	4000	500	125	1.51	7.26

Table 1 DNS dataset comprising smooth (S) and liner (L-C) cases where $C = \{S, T, E_{x-\chi}, E_{z-\chi}\}$ corresponds to the orifice configuration and χ is the number of ellipses per cavity. ΔU^+ is the Hama roughness function measured at $y^+ = 100$, where ℓ_T is the virtual origin shift. Simulations are performed in a computational box with dimensions $L_x \times L_y \times L_z = 3\delta \times 2(\delta + h) \times 1.5\delta$. d_x and d_z are the lengths of the streamwise and spanwise axes of the orifices. For cases L-S and L-T, $d_x^+ = d_z^+$. Δx^+ and Δz^+ are the viscous-scaled mesh spacing in the streamwise and spanwise direction, and $\Delta y^+_{\min}$ is the minimum mesh spacing in the wall-normal direction.

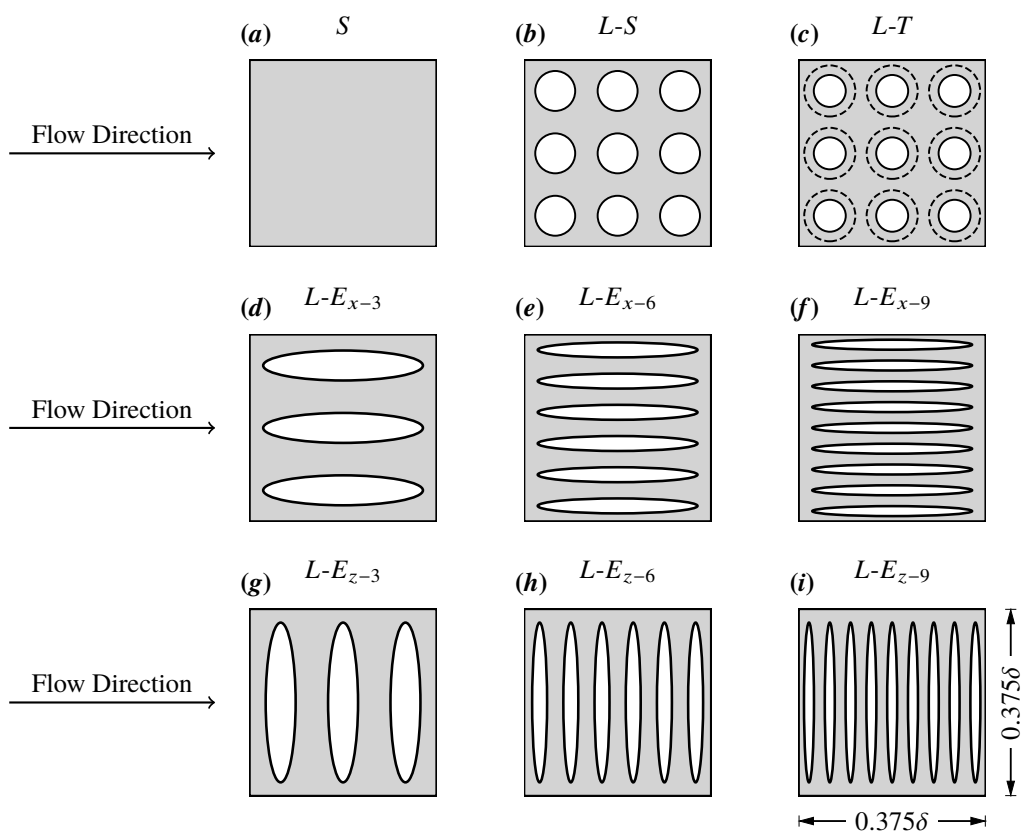

Fig. 2 Orifice configurations considered. All liner cases, except for case L_T have a top surface open area ratio of $\sigma = 0.322$. All liner cases are such that the total volume of the perforations is equal to $V_o = 9\pi d_s^2 t/4$, where d_s is the diameter of the baseline orifice configurations and $t = d_s$ is the thickness of the facesheet that is constant for all cases.

Downloaded by Technische Universiteit Delft on July 16, 2024 | http://arc.aiaa.org | DOI: 10.2514/6.2024-3282

II. Methodology

A. Test Setup

We solve the compressible Navier–Stokes equations in a plane channel flow configuration using the solver STREAmS [14, 15]. The computational domain is a rectangular box of size $L_x \times L_y \times L_z = 3\delta \times 2(\delta + h) \times 1.5\delta$, where δ is the channel half-width, h is the cavity depth, and x, y, z denote the streamwise, wall-normal and spanwise directions, respectively. Liner flow cases are complemented by a smooth-wall simulation at approximately the same friction Reynolds number and the same domain size. The simulations are performed at bulk Mach number $M_b = u_b/c_w = 0.3$, where u_b is the bulk flow velocity and c_w is the speed of sound at the wall. A uniform body force Π is added in the streamwise direction and adjusted each time step to maintain a constant mass flow rate in the channel core. The acoustic liner geometry is handled using a ghost-point forcing immersed boundary method [16]. Both walls are covered by an array of 8×4 acoustic liner cavities, as illustrated in Fig. 1. Each cavity has a square cross-section with a side length $\lambda_c = 0.335\delta$ and depth $h = 0.5\delta$. The cavity walls have a thickness of 0.02δ. We use a uniform mesh spacing in the streamwise and spanwise directions. In the wall-normal direction, the mesh is clustered towards the wall and coarsened towards the backplate and the channel centre. A minimum of 26 mesh points are used to resolve the orifice diameter (or minor axis in the case of an ellipse). This resolution is well within the viscous spacing typically accepted in DNS, and it has been previously validated [11].

We wish to study the influence of orifice geometry on the aerodynamic and acoustic performance of a liner and compare it to the baseline configuration with circular straight holes that are common in most applications. For the baseline reference case, see Fig. 2 **(*b*)** we consider the geometry studied by Shahzad et al. [11] with porosity $\sigma = 0.322$, viscous-scaled diameter $d^+ = d/\delta_v \approx 40$ and a thickness to diameter ratio $t/d = 1$, where the orifice diameter for the baseline case is $d = 0.08\delta$.

B. Novel Configurations

The facesheet thickness and the cavity dimensions remain unchanged for all cases considered. The novel configurations proposed only differ in the orifice shape, size, and orientation. In an attempt to reduce the aerodynamic drag induced by acoustic liners, we we propose liner geometries that should be more efficient from an aerodynamic perspective and possibly retain the acoustic properties of the liner. We change the orifice geometry while keeping constant the resonance frequency of the resonators $\omega_r = c_w\sqrt{A/tV_c}$, where A is the plane area of the orifice, and V_c is the volume of the cavity. In this way, we aim to optimise the aerodynamic performance without compromising the acoustic properties.

We propose reducing the effective porosity at the top surface of the facesheet by a 'tapered-hole' configuration where the orifice has a smaller diameter at the top of the facesheet and a larger diameter at the bottom of the facesheet, such that the total volume of the orifice is constant and the resonance frequency of the liner, does not change. For the

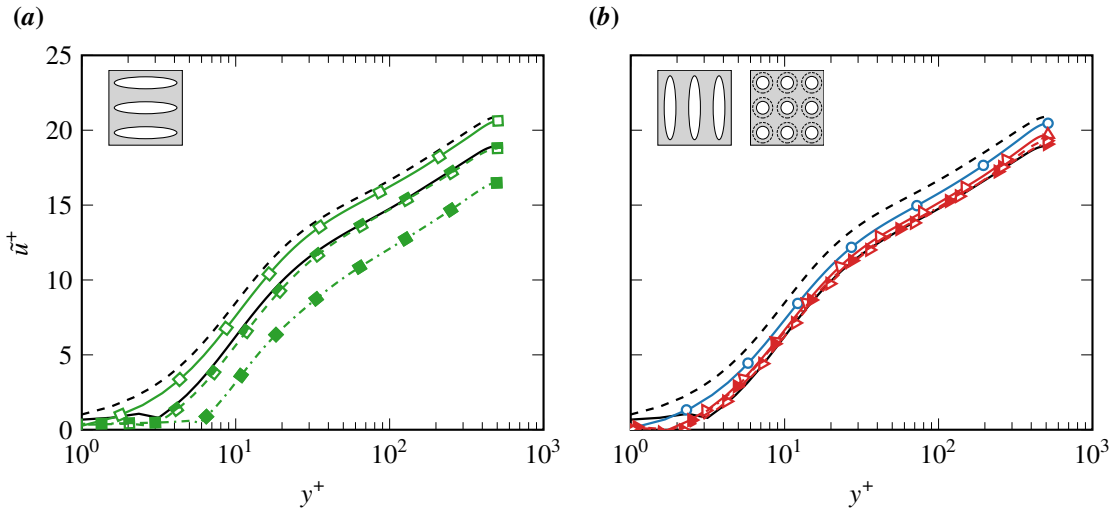

Fig. 3 Mean streamwise velocity for streamwise-oriented ellipses (*a*) and for spanwise-oriented ellipses and tapered circular holes (*b*). Novel geometries are compared to the smooth wall flow case (dashed black line without symbols) and to the baseline liner flow case (solid black line without symbols). The novel liner flow cases have the following line style: L-T (circles), L-$E_{x-\chi}$ (squares) and L-$E_{z-\chi}$ (triangles). Different line types with symbols indicate the number of orifices per cavity: $\chi = 3$ (dash-dotted line with filled symbols), $\chi = 6$ (dashed line with half-filled symbols) and $\chi = 9$ (solid line with empty symbols).

considered case (case L-T) the orifice diameter increases continuously from $d = 0.064\delta$ at the top of the facesheet to $d = 0.1024\delta$ at the bottom of the facesheet. We also propose elliptical orifices, that have the same porosity as the baseline liner, i.e. $\sigma = 0.322$. The major axis of the ellipse is fixed at $a = 0.32\delta$ and the minor axis is calculated by assuming a constant porosity and depends on the number of orifices per cavity. These ellipses can be oriented in the streamwise or spanwise direction. The geometries considered are shown in Fig. 2, and details of all flow cases are reported in Table 1. The naming of the flow cases is as follows: we use the letter S for the smooth wall case and L-C for the liner cases, where $C = \{S, T, E_{x-\chi}, E_{z-\chi}\}$ refers to the specific liner flow case. In particular, S, T, $E_{x-\chi}$ and $E_{z-\chi}$ are the baseline liner with straight orifice, tapered-orifice liner, streamwise-oriented ellipses and spanwise-oriented ellipses, respectively, and χ is the number of ellipses per cavity.

III. Results

A. Aerodynamic Drag

Figure 3 shows the mean streamwise velocity profiles for all flow cases, where we note a downward shift compared to the smooth wall (ΔU^+), indicating that all cases increase drag. However, several liner geometries exhibit a lower ΔU^+ compared to the baseline case, demonstrating that modifying the orifice shape can result in a lower added drag.

Some elliptical orifice configurations show potential for decreasing the added drag. However, this depends both on the ellipse dimensions and orientation. We observe a clear trend where narrowing the elliptical slots reduces the added

Downloaded by Technische Universiteit Delft on July 16, 2024 | http://arc.aiaa.org | DOI: 10.2514/6.2024-3282

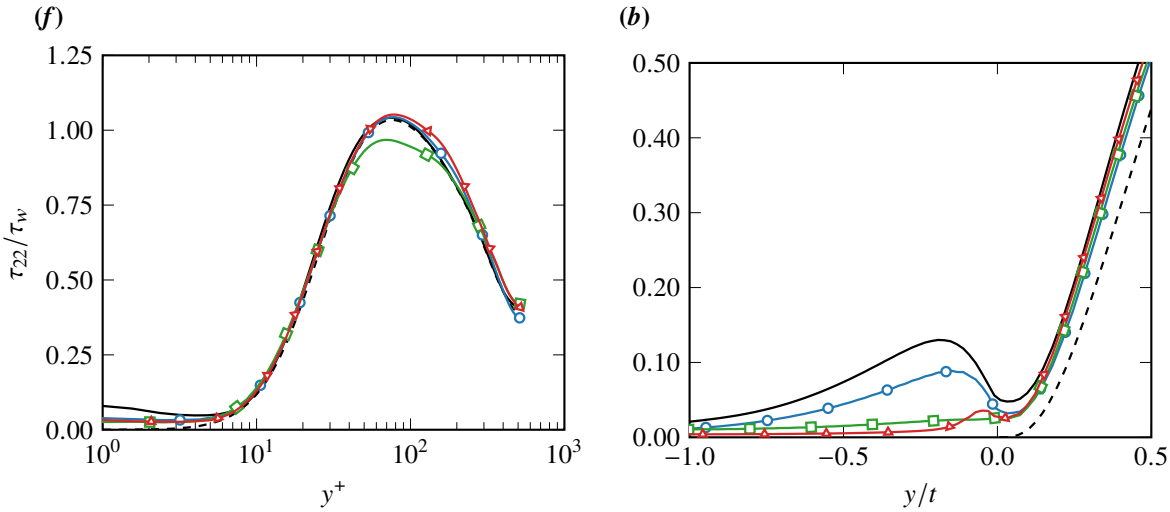

Fig. 4 Wall normal Reynolds stress τ_{22}, as a function of the viscous-scaled wall distance (*a*) and as a function of y/t (*b*), where t is the plate thickness, for smooth wall flow case (dashed line without symbols), the baseline liner flow case (solid line without symbols) and novel liner flow cases L-T (circles), L-E_{x-9} (squares) and L-E_{z-9} (triangles).

drag, independently from the orientation of the ellipses. For streamwise-oriented slots, the spanwise gap relates to the drag variation, and the narrow orifices of flow case L-E_{x-9} lead to a substantially lower drag than the baseline case, whereas the wider slots of case L-E_{x-3} result in a massive drag increase. ΔU^+ is less sensitive to the size of slots when the major axis is aligned with the spanwise direction. In this case, we find the same or a marginally lower drag than the baseline liner. These findings confirm the experiments of Howerton and Jones [13] who observed lower drag for spanwise-oriented rectangular slots. They found that streamwise-oriented rectangular slots increased drag compared to the baseline case, however, they did not investigate the effect of slot size. The tapered orifice also decreases drag compared to the baseline case. In this case, the improved performance can be traced back to the reduced superficial porosity experienced by the flow.

In a previous study, we related the added drag induced by acoustic liners to the wall-normal velocity fluctuations [11]. We show the wall-normal Reynolds stress components τ_{22} in Fig. 4 and 5. It is clear that the wall-normal velocity fluctuations are not zero, irrespective of the case considered, above and below the facesheet. We find that flow cases that exhibit lower drag than the baseline liner show lower wall-normal velocity fluctuations in the near-wall region and below the facesheet, Fig. 4. The converse is true for cases that increase the added drag, Fig. 5.

B. Acoustic Attenuation

We have studied the aerodynamic drag of different orifice configurations and have identified several geometries that induce lower drag compared to the baseline liner with circular orifices. As acoustic liners are used to reduce engine noise, it is imperative to also test their acoustic performance. In order to do so, we study the noise attenuation properties

Downloaded by Technische Universiteit Delft on July 16, 2024 | http://arc.aiaa.org | DOI: 10.2514/6.2024-3282

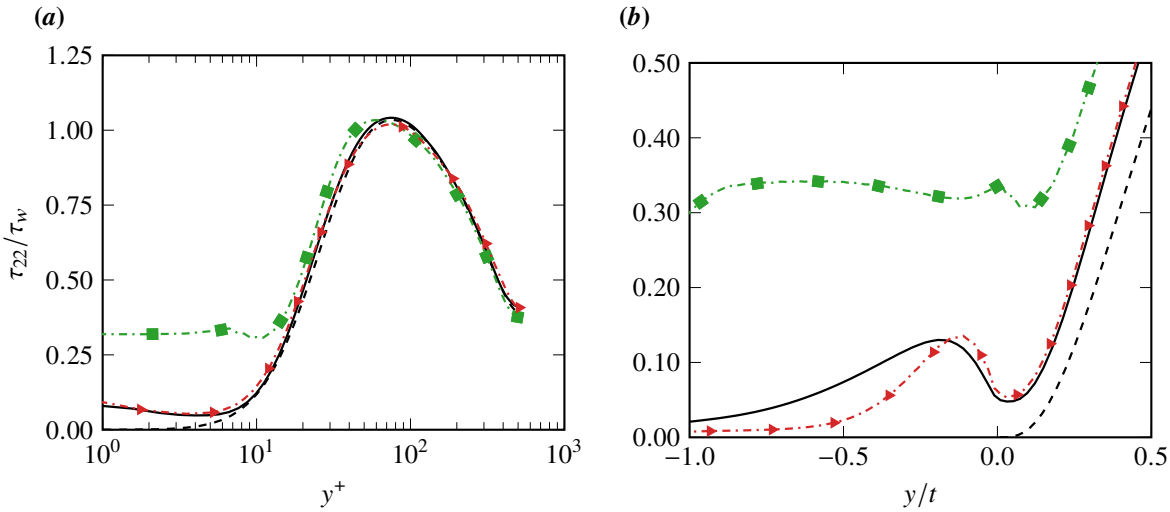

Fig. 5 Wall normal Reynolds stress τ_{22}, as a function of the viscous-scaled wall distance (*a*) and as a function of y/t (*b*), where t is the plate thickness, for smooth wall flow case (dashed line without symbols), the baseline liner flow case (solid line without symbols) and novel liner flow cases L-E_{x-3} (squares) and L-E_{z-3} (triangles).

of these novel configurations in the absence of grazing flow. A complete picture of the noise attenuation properties of aerodynamically optimised acoustic liner geometries would require including the influence of grazing flow. However, studies of acoustic liners without grazing flow have been extensively used to provide an initial estimation of their acoustic performance [17–19]. Simulations are performed in a channel of size $L_x \times L_y \times L_z = 1250d \times (25d + h) \times 4.69d$, where d is the orifice diameter of the baseline liner and $h = 6.25d$ is the depth of the liner. The spanwise domain size corresponds to a single cavity, and periodic boundary conditions are applied in the spanwise direction. We apply no-slip isothermal boundary conditions on the top and bottom walls and place acoustic liners at the bottom wall of the channel. An array of 40×1 acoustic liner cavities is placed between $x_s = 500d$ and $x_e = 687.5d$. The geometries of the liners are the same as those considered when studying the aerodynamic performance. At the inflow, an acoustic wave with a 130dB sound pressure level (SPL) is introduced into the domain with a frequency equal to the resonance frequency of the orifices $f \approx 0.028c/d$. We perform simulations at a Reynolds number $Re_c = 800$ based on the orifice diameter and speed of sound. We verified that, while the absolute sound attenuation of these liners changes, the relative sound attenuation, compared to the baseline acoustic liner, does not depend on the Reynolds number.

Figure 6 shows an instantaneous snapshot of the pressure for the smooth wall case and the baseline liner. As the frequency of the acoustic wave is tuned to the resonant frequency of the liner, we see a significant attenuation of the acoustic wave over the liner. The amplitude of the pressure fluctuations towards the end of the acoustic liner is much lower than over the smooth wall, where the fluid viscosity is the only dissipative mechanism.

Figure 7 compares the SPL evolution of the acoustic wave for all the liner configurations and the smooth wall. Although there is a clear SPL reduction for all configurations as compared to the smooth wall, some geometries perform

Downloaded by Technische Universiteit Delft on July 16, 2024 | http://arc.aiaa.org | DOI: 10.2514/6.2024-3282

Downloaded by Technische Universiteit Delft on July 16, 2024 | http://arc.aiaa.org | DOI: 10.2514/6.2024-3282

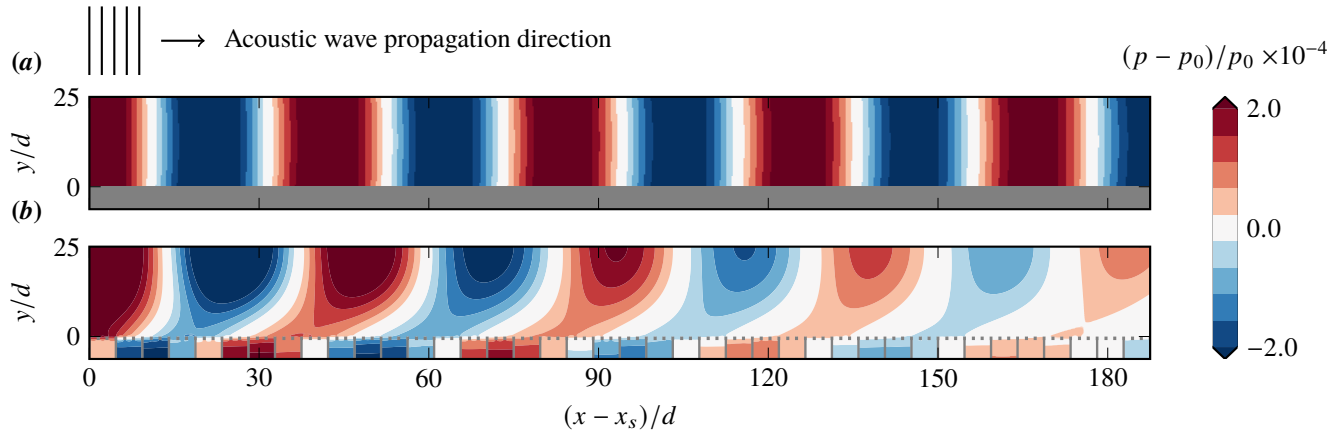

Fig. 6 Instantaneous pressure fluctuations over the smooth wall (*a*) and the baseline liner (*b*). p_0 is the reference thermodynamic pressure. Sound propagation direction is from left to right. x_s is the streamwise location where the liners start.

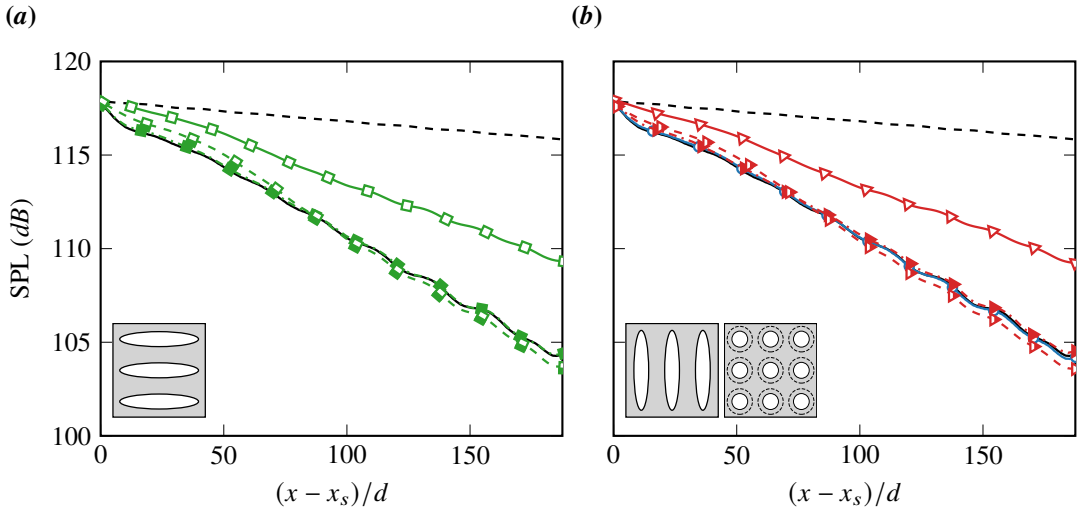

Fig. 7 Sound pressure level as a function of the streamwise distance from the start of the liners for smooth wall flow case (dashed line without symbols), the baseline liner flow case (solid line without symbols) and novel liner flow cases L-T (circles), L-$E_{x-\chi}$ (squares) and L-$E_{z-\chi}$ (triangles). Different line types with symbols indicate the number of orifices per cavity: $\chi = 3$ (dash-dotted line with filled symbols), $\chi = 6$ (dashed line with half-filled symbols) and $\chi = 9$ (solid line with empty symbols).

better than others when evaluated against the baseline liner.

Most configurations produce a very similar drop in the SPL over the domain, which confirms our design choices, except for cases L-E_{x-9} and L-E_{z-9}, which show a 50% lower sound attenuation than the baseline case. The narrow elliptical slots, that are effective for minimizing drag and improving the aerodynamic performance of the liners, appear to inhibit the interaction of the acoustic liner with the acoustic wave. The SPL loss in dB for cases L-E_{x-9} and L-E_{z-9} is approximately 50% lower than the baseline case. Some cases (L-T, L-E_{x-6} and L-E_{z-6}) produce a marginally higher SPL loss than the baseline configuration with case L-E_{x-6} offering an almost similar level of added drag as compared to the baseline case and case L-T offering slightly better aerodynamic performance. The tapered holes, therefore, improve not only the aerodynamic performance of the liner but also have a slightly better acoustic performance. The elliptical orifices, however, depending upon the width of the orifice, may or may not have a detrimental influence on acoustic noise attenuation.

IV. Conclusion

We have proposed several novel orifice geometries for acoustic liners, which reduce aerodynamic drag without compromising the acoustic performance. The idea behind the aerodynamically optimized geometries is based on flow physics, which allows us to restrict the vast parameter space that one could explore. The aerodynamic performance of the novel geometries is scrutinised based on Direct Numerical Simulations of fully resolved acoustic liner arrays in a turbulent channel flow. We find that tapered circular orifices minimize drag compared to a baseline acoustic liner by reducing the apparent porosity at the surface of the facesheet, whereas replacing the circular holes with elliptical slots can lead to a substantially lower drag if the minor axis of the ellipse is sufficiently thin in viscous units. We find that despite the very different configurations tested, all optimised geometries work by reducing the interaction of the flow above and below the surface of the facesheet, which is confirmed by the reduced wall-normal velocity fluctuations in the proximity of the facesheet. We also test the acoustic performance of the proposed liner configurations and find that the thin elliptical slots have a substantially reduced acoustic performance compared to a baseline liner; therefore, the improved aerodynamic benefit comes at the cost of lower noise reduction. The tapered hole configuration has slightly better noise attenuation properties than the baseline liner while offering substantially lower aerodynamic drag, and it is therefore superior both from an aerodynamic and acoustic perspective.

Acknowledgments

We acknowledge EuroHPC for awarding us access to Meluxina, at LuxProvide, Luxembourg.

References

[1] Sivian, L. J., "Acoustic Impedance of Small Orifices," *J. Acoust. Soc*, Vol. 7, No. 2, 1935, pp. 94–101.

Downloaded by Technische Universiteit Delft on July 16, 2024 | http://arc.aiaa.org | DOI: 10.2514/6.2024-3282

[2] Ingård, U., and Labate, S., "Acoustic Circulation Effects and the Nonlinear Impedance of Orifices," *J. Acoust. Soc. Am.*, Vol. 22, No. 2, 1950, pp. 211–218. https://doi.org/10.1121/1.1906591.

[3] Mann, A., Perot, F., Kim, M.-S., and Casalino, D., "Characterization of Acoustic Liners Absorption using a Lattice-Boltzmann Method," *AIAA paper 2013-2271*, 2013. https://doi.org/10.2514/6.2013-2271.

[4] Camussi, R., and Bennett, G. J., "Aeroacoustics research in Europe: The CEAS-ASC report on 2019 highlights," *J. Sound Vib.*, Vol. 484, 2020, p. 115540. https://doi.org/10.1016/j.jsv.2020.115540.

[5] Howerton, B. M., and Jones, M. G., "Acoustic liner drag: a parametric study of conventional configurations," *AIAA paper 2015-2230*, 2015. https://doi.org/10.2514/6.2015-2230.

[6] Howerton, B. M., and Jones, M. G., "A conventional liner acoustic/drag interaction benchmark database," *AIAA paper 2017-4190*, 2017. https://doi.org/10.2514/6.2017-4190.

[7] Gustavsson, J., Zhang, Y., Cattafesta, L. N., and Kreitzman, J. R., "Acoustic liner drag measurements," *AIAA paper 2019-2683*, 2019. https://doi.org/10.2514/6.2019-2683.c1.

[8] Dacome, G., Siebols, R., and Baars, W. J., "Inner-scaled Helmholtz resonators with grazing turbulent boundary layer flow," *arXiv:2308.07776 [physics]*, 2023.

[9] Scalo, C., Bodart, J., and Lele, S. K., "Compressible turbulent channel flow with impedance boundary conditions," *Phys. Fluids*, Vol. 27, No. 3, 2015, p. 035107. https://doi.org/10.1063/1.4914099.

[10] Zhang, Q., and Bodony, D. J., "Numerical investigation of a honeycomb liner grazed by laminar and turbulent boundary layers," *J. Fluid Mech.*, Vol. 792, 2016, pp. 936–980. https://doi.org/10.1017/jfm.2016.79.

[11] Shahzad, H., Hickel, S., and Modesti, D., "Turbulence and added drag over acoustic liners," *J. Fluid Mech.*, Vol. 965, 2023, p. A10.

[12] Shahzad, H., Hickel, S., and Modesti, D., "Permeability and turbulence over perforated plates," *Flow. Turbul. Combust.*, Vol. 109, No. 4, 2022, p. 1241–1254. https://doi.org/10.1007/s10494-022-00337-7.

[13] Howerton, B. M., and Jones, M. G., "Acoustic liner drag: measurements on novel facesheet perforate geometries," *AIAA paper 2016-2979*, 2016. https://doi.org/10.2514/6.2016-2979.

[14] Bernardini, M., Modesti, D., Salvadore, F., and Pirozzoli, S., "STREAmS: a high-fidelity accelerated solver for direct numerical simulation of compressible turbulent flows," *Comput. Phys. Commun.*, Vol. 263, 2021, p. 107906.

[15] Bernardini, M., Modesti, D., Salvadore, F., Sathyanarayana, S., Della Posta, G., and Pirozzoli, S., "STREAmS-2.0: Supersonic turbulent accelerated Navier-Stokes solver version 2.0," *Comput. Phys. Commun.*, Vol. 285, 2023, p. 108644. https://doi.org/https://doi.org/10.1016/j.cpc.2022.108644.

Downloaded by Technische Universiteit Delft on July 16, 2024 | http://arc.aiaa.org | DOI: 10.2514/6.2024-3282

[16] Vanna, F. D., Picano, F., and Benini, E., "A sharp-interface immersed boundary method for moving objects in compressible viscous flows," *Comput. Fluids*, Vol. 201, 2020, p. 104415. https://doi.org/10.1016/j.compfluid.2019.104415.

[17] Tam, C. K. W., Ju, H., Jones, M. G., Watson, W. R., and Parrott, T. L., "A computational and experimental study of resonators in three dimensions," *J. Sound Vib.*, Vol. 329, No. 24, 2010, pp. 5164–5193. https://doi.org/10.1016/j.jsv.2010.06.005.

[18] Zhang, Q., and Bodony, D. J., "Numerical investigation and modelling of acoustically excited flow through a circular orifice backed by a hexagonal cavity," *J. Fluid Mech.*, Vol. 693, 2012, pp. 367–401. https://doi.org/10.1017/jfm.2011.537.

[19] Schroeder, L., Spillere, A. M., Bonomo, L. A., da Silva, A. R., Avallone, F., and Cordioli, J. A., "Numerical Investigation of Acoustic Liners Experimental Techniques using a Lattice-Boltzmann Solver," *AIAA paper 2021-2144*, 2021. https://doi.org/10.2514/6.2021-2144.

Downloaded by Technische Universiteit Delft on July 16, 2024 | http://arc.aiaa.org | DOI: 10.2514/6.2024-3282